

Histopathology of diffusion imaging abnormalities in cerebral amyloid angiopathy

Susanne J. van Veluw, PhD,* Yael D. Reijmer, PhD,* Andre J. van der Kouwe, PhD, Andreas Charidimou, MD, PhD, Grace A. Riley, Alexander Leemans, PhD, Brian J. Bacskai, PhD, Matthew P. Frosch, MD, PhD, Anand Viswanathan, MD, PhD, Steven M. Greenberg, MD, PhD

Correspondence

Dr. van Veluw
svanveluw@
mgh.harvard.edu

Neurology® 2019;92:e933-e943. doi:10.1212/WNL.00000000000007005

Objective

We sought to determine the underlying mechanism for altered white matter diffusion tensor imaging (DTI) measures at the histopathologic level in patients with cerebral amyloid angiopathy (CAA).

Methods

Formalin-fixed intact hemispheres from 9 CAA cases and 2 elderly controls were scanned at 3-tesla MRI, including a diffusion-weighted sequence. DTI measures (i.e., fractional anisotropy [FA] and mean diffusivity [MD]) and histopathology measures were obtained from 2 tracts: the anterior thalamic radiation and inferior longitudinal fasciculus.

Results

FA was reduced in both tracts and MD was increased in cases with CAA compared to controls. Regional FA was significantly correlated with tissue rarefaction, myelin density, axonal density, and white matter microinfarcts. MD correlated significantly with tissue rarefaction, myelin density, and white matter microinfarcts, but not axonal density. FA and MD did not correlate with oligodendrocytes, astrocytes, or gliosis. Multivariate analysis revealed that tissue rarefaction ($\beta = -0.32 \pm 0.12$, $p = 0.009$) and axonal density ($\beta = 0.25 \pm 0.12$, $p = 0.04$) were both independently associated with FA, whereas myelin density was independently associated with MD ($\beta = -0.32 \pm 0.12$, $p = 0.013$). Finally, we found an association between increased MD in the frontal white matter and CAA severity in the frontal cortex ($p = 0.035$).

Conclusions

These results suggest that overall tissue loss, and in particular axonal and myelin loss, are major components underlying CAA-related alterations in DTI properties observed in living patients. The findings allow for a more mechanistic interpretation of DTI parameters in small vessel disease and for mechanism-based selection of candidate treatments to prevent vascular cognitive impairment.

*These authors contributed equally to this work.

From the J. Philip Kistler Stroke Research Center, Department of Neurology (S.J.v.V., Y.D.R., A.C., G.A.R., A.V., S.M.G.), and Neuropathology Service, C.S. Kubik Laboratory for Neuropathology (M.P.F.), Massachusetts General Hospital and Harvard Medical School, Boston; MassGeneral Institute for Neurodegenerative Disease (S.J.v.V., B.J.B., M.P.F.), Charlestown Navy Yard, MA; Department of Neurology, Brain Center Rudolf Magnus (Y.D.R.), and Image Sciences Institute (A.L.), University Medical Center Utrecht, Utrecht University, the Netherlands; and Athinoula A. Martinos Center for Biomedical Imaging (A.J.v.d.K.), Department of Radiology, Massachusetts General Hospital, Charlestown.

Go to Neurology.org/N for full disclosures. Funding information and disclosures deemed relevant by the authors, if any, are provided at the end of the article.

Glossary

AD = axial diffusivity; **ATR** = anterior thalamic radiation; **CAA** = cerebral amyloid angiopathy; **DTI** = diffusion tensor imaging; **FA** = fractional anisotropy; **GFAP** = glial fibrillary acidic protein; **H&E** = hematoxylin & eosin; **ILF** = inferior longitudinal fasciculus; **LFB&H** = Luxol fast blue & hematoxylin; **MBP** = myelin basic protein; **MD** = mean diffusivity; **MGH** = Massachusetts General Hospital; **NF200** = neurofilament 200; **RD** = radial diffusivity; **ROI** = region of interest; **SVD** = small vessel disease; **TBS** = tris-buffered saline; **TE** = echo time; **TR** = repetition time; **True FISP** = true fast imaging with steady-state free precession.

Cerebral small vessel disease (SVD) is a major contributor to cognitive dysfunction in older individuals.^{1,2} Despite the high prevalence of SVD, we do not have a clear understanding of the underlying pathophysiology of SVD vascular impairment and its downstream effects on the surrounding brain tissue.^{3,4} Recent findings from diffusion tensor imaging (DTI) studies suggest that microscopic abnormalities in the white matter are a sensitive and clinically meaningful marker of SVD-related brain injury.^{2,5–7} DTI allows for in vivo assessment of tissue microstructure integrity by characterizing the diffusion profile of water molecules.⁸ Common DTI measures are fractional anisotropy (FA) and mean diffusivity (MD), which quantify the directional dependency and degree of water diffusion within a voxel. Abnormal FA and MD values are assumed to indicate alterations in axonal and myelin density⁸ but have also been related to other forms of tissue injury⁹ and to non-disease-related variations in tissue structure.^{10–12} Most insights into the histopathologic underpinnings of FA and MD are derived from animal studies. For these reasons, the structural correlates and pathogenic mechanism underlying abnormal DTI values in patients with SVD remain unidentified, making clinical interpretation challenging.

We therefore explored the underlying histopathology of white matter DTI measures detected with ex vivo MRI in intact hemispheres of decedents with cerebral amyloid angiopathy (CAA), a common and well-defined form of SVD.¹³ We hypothesized that previously observed alterations in white matter DTI measures on in vivo MRI^{14–16} correlate with specific histologic measures of white matter injury and are associated with cortical CAA severity.

Methods

Brain samples

Intact brains were received through an ongoing postmortem brain MRI study for the evaluation of MRI markers and their underlying histopathology in the context of CAA. All cases included in the study were from patients diagnosed with possible or probable CAA during life¹³ who either donated their brain for research or came to autopsy through the Massachusetts General Hospital (MGH) neuropathology service. The clinical diagnosis was confirmed by the patient's medical records and available clinical MRI or CT obtained during life, and validated by neuropathologic examination of the brain postmortem. At autopsy, the brains were removed

and fixed in 10% formalin for at least 3 weeks. After fixation, the hemispheres were separated by a single midsagittal cut. The hemisphere that was least affected by large intracerebral hemorrhage was used for ex vivo MRI scanning. The other hemisphere was processed to undergo standard neuropathologic examination to obtain a formal neuropathologic diagnosis by a board-certified neuropathologist. The hemisphere to undergo ex vivo MRI was packed in a plastic bag, filled with periodate-lysine-paraformaldehyde fixative, and vacuum sealed. The packed hemispheres were held at 4°C until the day before the MRI, when they were kept at room temperature. Any remaining air bubbles were removed, followed by resealing of the bag.

Two autopsy cases, without any neurologic conditions or brain lesions that came through the MGH neuropathology service were added as control cases. One hemisphere was selected at random and processed identically.

Standard protocol approvals, registrations, and patient consents

The MGH institutional review board approved this study. Informed consent was obtained from the next of kin or other legal representative prior to brain removal.

Ex vivo MRI scanning

Each packed hemisphere was placed in a 32-channel head coil of a 3-tesla MRI scanner (Siemens MAGNETOM Trio; Siemens Healthcare, Erlangen, Germany) and scanned with an overnight protocol (total scan time approximately 14 hours). Each hemisphere was positioned within the head coil in a similar fashion, with the cerebellum inserted first and the lateral side of the brain facing down. Padding was used to prevent motion during scanning. The ex vivo MRI scan protocol included the following sequences: (1) T2-weighted turbo-spin echo (voxel size $500 \times 500 \times 500 \mu\text{m}^3$; echo time (TE) 61 milliseconds (ms); repetition time (TR) 1,800 ms; flip angle 150°; turbo factor 15; receiver bandwidth 131 Hz/Px; total scan time 3 hours 8 minutes 11 seconds); (2) gradient-echo fast low angle shot (voxel size $500 \times 500 \times 500 \mu\text{m}^3$; TE₁ 4.49 ms; TE₂ 11.02 ms; TR 20 ms; flip angle 10°, 20°, 30°; receiver bandwidth 160 Hz/Px; 2 averages; total scan time 119 minutes); (3) diffusion-weighted gradient-echo true fast imaging with steady-state free precession (True FISP) (voxel size $1 \times 1 \times 1 \text{ mm}^3$; 44 gradient directions with a b value of approximately $1,000 \text{ s/mm}^2$ and 8 b₀ images¹⁷; TE 23.89 ms; TR 29.77 ms; receiver

bandwidth 100 Hz/Px; total scan time 7 hours 51 minutes 55 seconds).

MRI analysis

The acquired scans were preprocessed in FreeSurfer (surfer.nmr.mgh.harvard.edu) to obtain 3-dimensional volumes.¹⁸

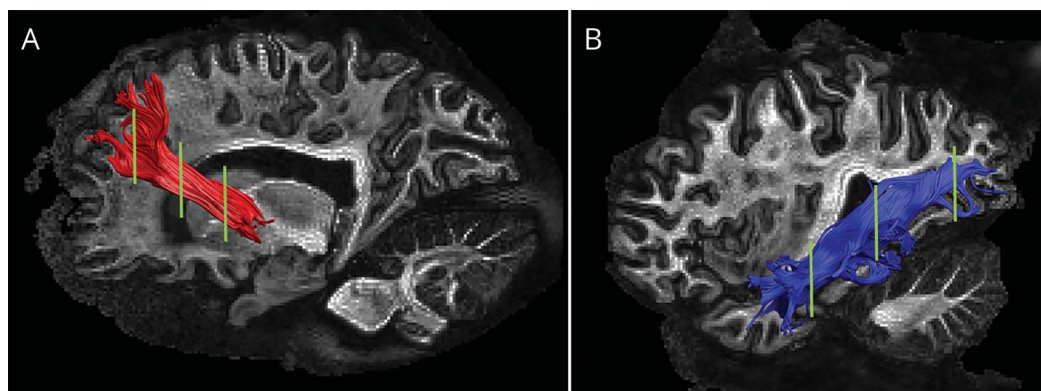
Diffusion-weighted True FISP scans were processed using ExploreDTI (exploredti.com).¹⁹ Images were corrected for diffusion signal drift,²⁰ movement, and eddy-current distortions.²¹ Diffusion tensors were calculated using weighted linear least squares.²² Deterministic streamline whole-brain fiber-tracking based on the principal eigenvector was performed, with seed samples distributed uniformly throughout the volume at 1-mm isotropic resolution.²³ Fiber tracts were terminated when they deflected at an angle of more than 30° or if they entered a voxel with an FA less than 0.10. Parameter settings for fiber tractography were optimized for the current dataset. From the whole-brain fiber tractography maps, 2 tracts of interest were delineated: the inferior longitudinal fasciculus (ILF), running between the occipital and temporal lobes, and the anterior thalamic radiation (ATR), running between the thalamus and the frontal cortex (figure 1). These tracts were selected because *in vivo* diffusion abnormalities in CAA have been shown to involve primarily occipital-temporal white matter connections (such as the ILF), and less often subcortical and frontal white matter connections (such as the ATR).¹⁵ In addition, the majority of ILF and ATR fibers have relatively low curvature, thereby simplifying reconstruction. Tracts were manually delineated based on a priori information on tract location^{24,25} by an experienced analyst (Y.D.R.) blinded to clinical information that could not be inferred from the scan. All tract reconstructions were visually inspected and spurious tracts were excluded. At the anterior, medial, and posterior parts of each tract, regions of interest (ROIs) of 3-mm thickness were selected that corresponded to the same

location as the samples selected for histopathology (figures 1 and 2). The mean FA, MD, axial diffusivity (AD), and radial diffusivity (RD) were calculated for the whole white matter tract and for each ROI. The inferior part of the ILF of one case was compromised due to a hemorrhage in the temporal lobe. The results did not change when excluding the ILF of this case from the analysis. We therefore report the results including data from the preserved parts of this case's ILF.

Sampling and histopathologic analysis

After scanning, each cerebral hemisphere was cut in 10-mm-thick coronal slabs. Seven predefined areas were sampled: 3 ROIs from the ATR, 3 ROIs from the ILF (figure 1), and 1 ROI from the parietal cortex. Each sample measured approximately $2 \times 1 \times 0.5 \text{ mm}^3$ to fit a standard tissue cassette. Next, the samples were processed and dehydrated through graded series of ethanol, embedded in paraffin, and cut in 6- μm -thick serial sections on a microtome. Adjacent sections were stained with hematoxylin & eosin (H&E) (to assess white matter microinfarcts) and Luxol fast blue & hematoxylin (LFB&H) (to assess tissue rarefaction and oligodendrocytes), following standard histology protocols. Bright-field immunohistochemistry was performed against β -amyloid (clone 6F/3D; Agilent Technologies, Inc., Santa Clara, CA) (to assess CAA and parenchymal plaques) and glial fibrillary acidic protein (GFAP) (G9269; Sigma-Aldrich, St. Louis, MO) (to assess gliosis, reactive astrocytes, and white matter microinfarcts) on neighboring sections, using standard immunohistochemistry protocols. Briefly, sections were deparaffinized in xylene and rehydrated through graded ethanol series. Endogenous peroxidase was quenched with 3% H_2O_2 for 20 minutes, followed by a 5-minute antigen retrieval step in formic acid. Next, sections were blocked in normal serum (from Vectastain ABC-HRP kits; Vector Laboratories, Burlingame, CA) and incubated with the primary antibody overnight at 4°C. The next day, sections were washed with tris-buffered saline (TBS), and

Figure 1 The anterior thalamic radiation and inferior longitudinal fasciculus



Depicted are sagittal projections of the anterior thalamic radiation (A) and inferior longitudinal fasciculus (B), reconstructed with fiber tractography. The green lines represent the ROIs within the tract at which diffusion tensor imaging values were extracted and at which tissue samples were taken for histopathologic analysis. They represent the anterior, medial, and posterior aspects of both tracts, and contain the frontal, temporal, and occipital cortices (for the quantification of cortical CAA pathology). Fractional anisotropy/mean diffusivity values of each ROI were related to histopathologic markers of white matter tissue injury and to ratings of cortical CAA severity on corresponding tissue sections. CAA = cerebral amyloid angiopathy; ROI = region of interest.

antibody labeling was visualized using a peroxidase-conjugated secondary reagent (from Vectastain ABC-HRP kits; Vector Laboratories) and DAB (3,3'-diaminobenzidine) as the chromogen (Vector Laboratories). Sections were briefly counterstained with hematoxylin, dehydrated and cleared in xylene, and coverslipped using Permount mounting medium. Finally, one additional neighboring section underwent fluorescent immunohistochemistry against myelin basic protein (MBP) (NE1019; EMD Millipore, Burlington, MA) and neurofilament (NF200, N4142; Sigma) to quantify myelin density, axonal density, and myelination fraction. Sections were deparaffinized in xylene and rehydrated through a graded ethanol series. Next, sections underwent antigen retrieval for 20 minutes in heated citrate buffer (pH approximately 6), permeabilization for 30 minutes with 0.5% Triton X-100 in TBS, blocking for 1 to 1.5 hours with 10% normal goat serum, and incubation with the primary antibody overnight at 4°C. The next day, sections were washed with TBS + 5% normal goat serum + 0.05% Triton X-100, followed by an incubation with fluorescent secondary antibodies for 1.5 hours (Alexa Fluor 488 and Cy3, respectively). Sections were coverslipped using Vectashield with DAPI (4',6-diamidino-2-phenylindole) (Vector Laboratories) as the mounting medium. A negative control was included by omitting the primary antibodies.

Image analysis

Each histopathologic section was scanned using the NanoZoomer whole slide scanner (Hamamatsu Photonics K.K., Hamamatsu City, Japan) with a 20× objective, and the obtained digital images were assessed with the software NDP.view (version 2.6.13; Hamamatsu Photonics K.K.). Settings, such as white balance and exposure time and gain for each channel (red, green, blue), in the case of fluorescent imaging, were kept the same for all sections to ensure standardized image acquisition. Cortical CAA severity was evaluated on the β -amyloid-stained sections taken from the frontal, parietal, temporal, and occipital cortex, following recent consensus criteria.²⁶ The scale ranged from 0 (no parenchymal CAA), 1 (scant vascular β -amyloid deposition), 2 (some circumferential β -amyloid), to 3 (widespread circumferential β -amyloid) for each section, resulting in a maximum cumulative score of 12. All white matter histopathologic measures were assessed within the 3 ROIs of the ATR and ILF (i.e., the anterior, medial, and posterior aspects of both tracts) (figure 1). For quantification, images were exported to ImageJ (Fiji app).²⁷ At 1.25× magnification, segments of the ATR or ILF were outlined on the LFB&H-stained sections, based on anatomical landmarks, by one of the authors (S.J.v.V.) blinded to DTI findings (figure 2). White matter tissue rarefaction was assessed on the LFB&H-stained sections at 1.25× magnification operationalized by calculating the mean brightness of the LFB&H signal within those segments using the /Analyze/Measure option in ImageJ. Individual oligodendrocytes, recognizable by their morphology, were counted within each segment on the LFB&H-stained sections at 40× using the cell-counter module in ImageJ. The total number of oligodendrocytes per segment was used as outcome measure

since all evaluated segments were of similar size. Degree of gliosis and number of reactive astrocytes were similarly assessed on the GFAP-stained sections at 40× magnification; degree of gliosis was operationalized by calculating the mean brightness of the GFAP signal, and individual reactive astrocytes were counted manually. Mean brightness of the MBP and NF200 fluorescent signal, reflecting myelin and axonal density, respectively, was measured in separate channels (i.e., green and red) at 40× magnification. Myelination fraction was calculated by taking the ratio between myelin density and axonal density. Finally, white matter microinfarcts were assessed on both H&E and GFAP-stained sections, in consensus with a board-certified experienced neuropathologist (M.P.F.).

Statistical analysis

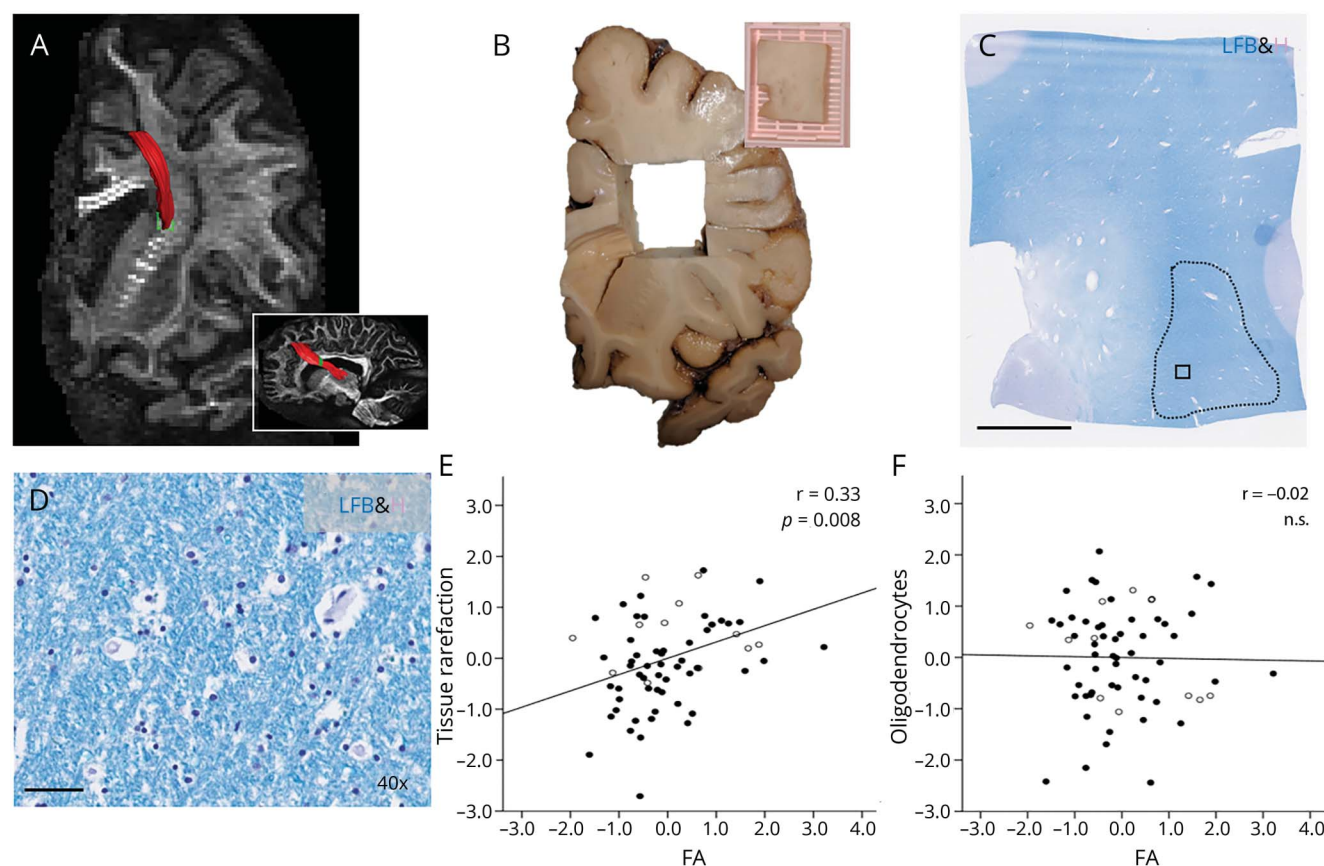
Ex vivo MRI-based FA and MD values of the ATR and ILF were compared between CAA cases and controls by calculating age-adjusted between-group differences with analysis of variance. Since sex was not related to any of the outcome measures, it was not included in our models. Between-group differences were expressed as effect sizes (SD units) in order to compare our findings to previous in vivo reports. An effect size of ≤ 0.2 is considered small, and ≥ 0.8 is considered large.²⁸

The association between DTI values and histopathology markers of white matter tissue injury were evaluated across all ROIs ($n = 66$) and ROIs from CAA cases only ($n = 54$) with linear mixed models in which we accounted for the shared variance between ROIs of the same case by including cases as random effect. Age was entered as covariate and group as fixed factor. Histopathology measures that were derived from different batches were adjusted for batch effect by regressing out the variance explained by batch with linear regression analysis before entering the variable in subsequent models. We also tested for a tract (ILF vs ATR) \times histopathology marker interaction effect on FA and MD. Next, all histopathology measures that were significantly associated with DTI values in univariate analyses were simultaneously entered in a multivariate linear mixed model to test whether these measures independently contributed to the DTI signal.

The association between DTI values and CAA severity in the overlying cortex was evaluated in the frontal and occipital parts of the brain by testing associations between the anterior portion of the ATR and superior frontal cortex and between the posterior portion of the ILF and occipital cortex. Because of the limited variance in the occipital CAA severity score (all CAA cases had moderate to severe CAA in occipital cortex), we chose the statistical approach used in a previous in vivo analysis,¹⁵ comparing frontal DTI values between CAA cases with moderate to severe CAA in frontal cortex (score 2–3; $n = 3$) to CAA cases without frontal CAA or with mild frontal CAA (score 0–1; $n = 6$) using an independent-samples *t* test.

Finally, we evaluated whether the identified histopathologic correlates of FA and MD differed between CAA cases and controls by calculating age-adjusted effect sizes.

Figure 2 Diffusion tensor imaging–white matter histopathology correlations



Depicted is the medial ROI of the anterior thalamic radiation in a case with cerebral amyloid angiopathy (A) and the corresponding area that was sampled for histopathologic analysis (B). Tissue rarefaction for each ROI was calculated on the LFB&H-stained section at 1.25 \times magnification within the outlined area in the white matter (C). Other histopathology measures, such as oligodendrocyte count, were assessed at 40 \times magnification (D). Panel D corresponds to the area indicated with a square in C. Across ROIs, FA was significantly correlated with tissue rarefaction (E), but not with oligodendrocyte count (F). Black dots indicate ROIs from cases with cerebral amyloid angiopathy and white dots from controls. Variables are presented as age-adjusted standardized residuals. Scale bar in C indicates 5 mm; scale bar in D indicates 50 μ m. FA = fractional anisotropy; LFB&H = Luxol fast blue & hematoxylin; n.s. = not significant; ROI = region of interest.

Data availability

All the relevant methods and data resulting from this study are reported in the article or in data available from Dryad (table e-1, doi.org/10.5061/dryad.j51d02h).

Results

General findings

The brains of 9 CAA cases (mean age at death 70 years [range: 64–81]; 7 males, 2 females) and 2 elderly controls (a 95-year-old female and a 90-year-old male) were included in this study (table 1). All cases met the Boston criteria for definite CAA,¹³ and the controls had no CAA on neuropathologic examination.

Between-group differences in DTI measures

The FA of both the ATR and ILF was reduced by 1.9 SD in CAA cases compared to controls after adjusting for age (table 2). The MD of the ATR was increased by 0.3 SD and the MD of the ILF by 1.1 SD in CAA cases compared to

controls. Post hoc analysis showed that the changes in FA and MD were caused by a greater increase in RD, i.e., diffusion direction perpendicular to the tract (effect size ATR 0.6, ILF 1.32 SD) than AD, i.e., diffusion parallel to the tract (ATR 0.1, ILF 0.8 SD). Adjusting for total ABC score, reflecting the burden of Alzheimer disease pathology, did not mitigate these between-group differences (effect size ATR: FA -1.51 , MD 2.61 SD, and ILF: FA -2.46 , MD 1.18 SD).

DTI–white matter histopathology correlations

FA and MD values of each ROI were associated with several histopathologic markers of white matter injury in the corresponding ROI (table 3).

Decreased FA and increased MD were associated with an increase in tissue rarefaction, as quantified on the LFB&H sections at 1.25 \times (figure 2). Decreased FA and increased MD were also associated with lower myelin density as measured on the MBP sections at 40 \times (table 3, figure 3). FA and MD values were not associated with the number of oligodendrocytes as counted on the LFB&H sections at 40 \times , however

Table 1 Case characteristics

Study ID	Age at death, y	Sex	Hemisphere	Postmortem interval, h	Fixation duration, d	CAA severity on pathology (cumulative score) ^a	Other neuropathologic observations ^b
Cases							
1	80	M	R	Unknown	476	5	A3B3C2
2	70	M	L	16	377	9	A3B3C1, moderate hypertensive vasculopathy
3	76	M	R	27	43	7	A3B3C2, arteriolosclerosis
4	65	M	L	14	498	7	A3B1C2
5	81	M	R	Unknown	69	5	A3B2C2, moderate arteriolosclerosis
6	70	F	L	Unknown	71	6	NA
7	67	M	L	Unknown	50	10	A3B3C2
8	69	M	L	36	27	10	A3B1C2, mild arteriolosclerosis
9	64	F	R	30	67	8	A3B2C3
Controls							
1	90	M	L	6	58	0	A2B1C2, mild hypertensive disease
2	95	F	L	4	45	0	A1B2C0

Abbreviations: CAA = cerebral amyloid angiopathy; ID = identification; NA = not available. Leptomeningeal CAA severity was not considered.

^a A cumulative score for cortical CAA severity was calculated by taking the sum of each score as measured on the β -amyloid-stained sections obtained from the frontal, parietal, temporal, and occipital cortices. The scale ranged from 0 to 3 for each section, resulting in a maximum cumulative score of 12.²⁶

^b Extracted from the autopsy report based on neuropathologic observations in the other hemisphere. ABC score reflects the National Institute on Aging-Alzheimer Association score for Alzheimer disease neuropathologic changes.

(figure 2). In addition, we found an association between decreased FA and decreased axonal density (NF200). Myelination fraction (i.e., the ratio of myelin density to axonal density) was associated with both FA and MD. Post hoc analysis with measures of radial and axial diffusion showed that tissue rarefaction and axonal density were associated with RD, but not AD. By contrast, myelin density was associated with both RD and AD.

No significant correlations were found between DTI measures and GFAP markers (i.e., gliosis or reactive astrocyte count) (table 3, figure 3).

Regression coefficients did not notably change when considering ROIs from CAA cases only (data not shown). Stratifying significant associations by tract showed that histology-DTI associations tended to be stronger for ROIs of

Table 2 Ex vivo diffusion MRI findings

	Controls (n = 2)	CAA (n = 9)	Age-adjusted effect size	p Value
ATR (frontal white matter tract)				
FA	0.36 (0.33–0.39)	0.31 ± 0.03	–1.86	0.17
MD	0.33 (0.32–0.34)	0.34 ± 0.04	0.32	0.84
ILF (posterior white matter tract)				
FA	0.40 (0.37–0.43)	0.28 ± 0.03	–1.90	0.06
MD	0.29 (0.23–0.35)	0.38 ± 0.07	1.13	0.44

Abbreviations: ATR = anterior thalamic radiation; CAA = cerebral amyloid angiopathy; FA = fractional anisotropy; ILF = inferior longitudinal fasciculus; MD = mean diffusivity ($\times 10^{-3}$ mm²/s).

Data represent means \pm SD or range. Relatively low FA and high MD indicate abnormal diffusion. Effect sizes are adjusted for age. Effect size of ≥ 0.8 is considered large and ≤ 0.2 is considered small.²⁸

Table 3 Correlations between ex vivo diffusion values and histology markers of white matter injury

Histopathology marker	FA	MD
Tissue rarefaction	$\beta = -0.31 \pm 0.11$	$\beta = 0.30 \pm 0.12$
LFB&H (1.25 \times)	$p = 0.008^a$	$p = 0.014$
Myelin density	$\beta = 0.38 \pm 0.12$	$\beta = -0.50 \pm 0.12$
MBP (40 \times)	$p = 0.002^b$	$p < 0.001$
Axonal density	$\beta = 0.31 \pm 0.11$	$\beta = -0.21 \pm 0.12$
NF200 (40 \times)	$p = 0.007^a$	NS
Myelination fraction	$\beta = 0.27 \pm 0.13$	$\beta = -0.46 \pm 0.13$
MBP/NF200 (40 \times)	$p = 0.047^b$	$p < 0.001$
Gliosis	$\beta = -0.05 \pm 0.12$	$\beta = 0.23 \pm 0.12$
GFAP (40 \times)	NS	NS
Reactive astrocytes	$\beta = 0.08 \pm 0.12$	$\beta = -0.003 \pm 0.13$
GFAP (40 \times)	NS	NS
Oligodendrocytes	$\beta = -0.03 \pm 0.12$	$\beta = -0.09 \pm 0.12$
LFB&H (40 \times)	NS	NS

Abbreviations: FA = fractional anisotropy; GFAP = glial fibrillary acidic protein; LFB&H = Luxol fast blue & hematoxylin; MBP = myelin basic protein; MD = mean diffusivity; NF200 = neurofilament 200; NS = not significant.

Adjusted standardized regression coefficients \pm SE across all regions of interest ($n = 66$). Relatively low FA and high MD indicate abnormal diffusion. Higher histopathology values indicate more rarefaction, higher myelin density, higher axonal density, more gliosis, more reactive astrocytes, and more oligodendrocytes, respectively. Myelination fraction = MBP/NF200.

^a Correlation coefficients were significant for radial but not axial diffusivity. ^b Correlation coefficients were similar for radial and axial diffusivity.

the ILF than of the ATR (data available from Dryad, table e-1, doi.org/10.5061/dryad.j51d02h). When we additionally controlled for fixation duration (i.e., time between death and scanning, table 1) in our models, the results did not notably change.

Microinfarcts in the white matter were detected in the anterior and medial ROI of the ILF in 3 cases with CAA (figure 3). The FA was lower and MD was higher in those 3 microinfarct-containing ROIs compared to the same ILF ROIs of CAA cases without microinfarcts ($n = 12$) (between-group difference \pm SEM: FA -0.07 ± 0.03 , $p = 0.02$, and MD 0.10 ± 0.04 , $p = 0.03$).

Multivariate analyses

The individual histopathology measures correlated with DTI parameters in univariate analyses (i.e., tissue rarefaction, myelin density, and axonal density) were simultaneously entered in a multivariate model to test for their independent contribution to the DTI signal. None of these measures were collinear (Pearson $r < 0.4$). Tissue rarefaction and axonal density were both independently associated with FA (LFB&H: $\beta = -0.32 \pm 0.12$, $p = 0.009$; NF200: $\beta = 0.25 \pm 0.12$, $p = 0.04$), whereas myelin density was independently

associated with MD (MBP: $\beta = -0.32 \pm 0.12$, $p = 0.013$). Similar results were found in CAA patients only (data not shown). In a separate multivariate model including ROIs evaluated for white matter microinfarcts ($n = 15$), microinfarcts were independently associated with FA ($\beta = -0.60 \pm 0.22$, $p = 0.018$) and MD ($\beta = 1.47 \pm 0.37$, $p < 0.001$).

DTI-CAA severity correlations

CAA cases with moderate to severe CAA in frontal cortex ($n = 3$) had increased MD in the frontal white matter (between-group difference \pm SEM: $0.05 \pm 0.02 \times 10^{-3} \text{ mm}^2/\text{s}$, $p = 0.035$) but not in the occipital white matter (MD: 0.007 ± 0.07 , $p = 0.93$) compared to CAA cases with no or mild CAA in frontal cortex ($n = 6$) (figure 4). Correspondingly, all CAA cases had moderate to severe CAA in occipital cortex. Of note, all 9 CAA cases exhibited parenchymal β -amyloid plaques in frontal cortex, which excluded parenchymal plaque load as a possible confounder in this analysis.

Between-group differences in white matter histopathology markers

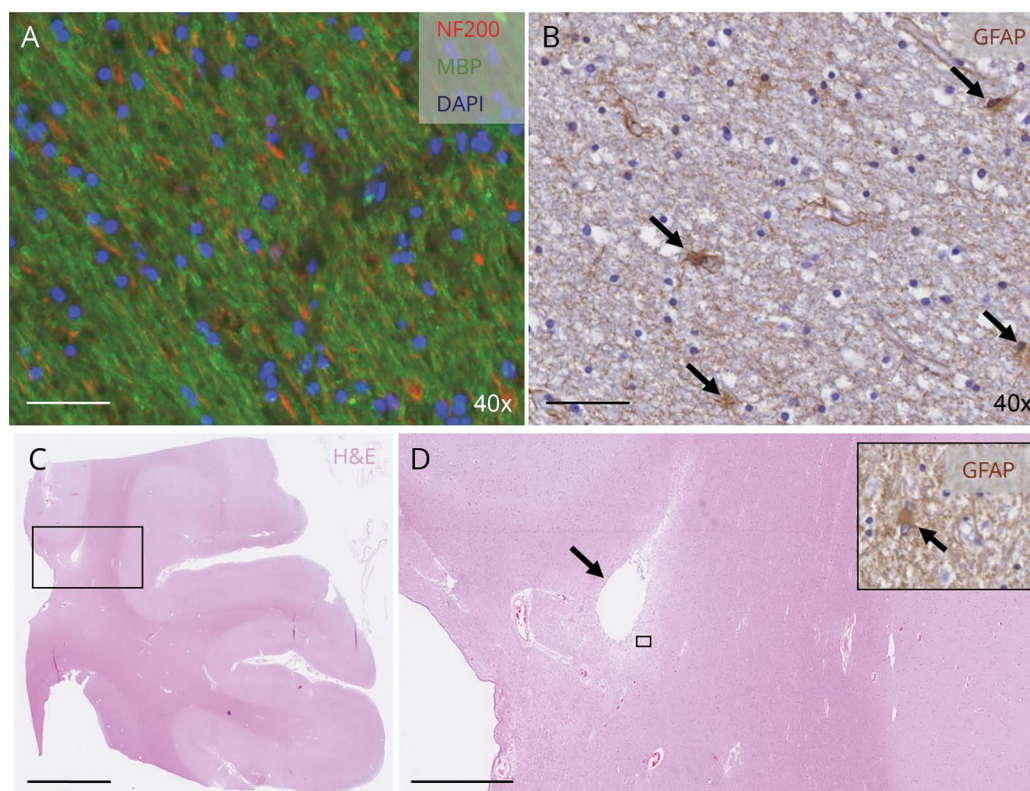
Finally, we explored whether the white matter histopathology measures that significantly correlated with FA and MD in multivariate models differed between cases with CAA and the 2 controls. Cases with CAA had greater tissue rarefaction compared to controls, especially in the ILF (between-group difference in z scores \pm SEM: ATR 0.65 ± 1.08 , ILF 1.09 ± 1.02). Furthermore, myelin density but not axonal density was lower in cases with CAA compared to controls in both white matter tracts (between-group difference in z scores \pm SEM: ATR -1.16 ± 1.45 , ILF -1.07 ± 0.86).

Discussion

There are several key findings from this study. First, we demonstrated changes in DTI measures (i.e., decreased FA, increased MD) on ex vivo MRI, corresponding with previously demonstrated changes in these same DTI measures on in vivo MRI in patients with CAA. Second, we found that DTI measures were associated with local markers of white matter tissue integrity, myelin, and axonal density, but not with markers of gliosis or with oligodendrocyte counts. Abnormal DTI values in the posterior white matter were also associated with the presence of microinfarcts in the corresponding ROIs, although numbers were low. Finally, we found that higher CAA burden in the frontal cortex was associated with increased MD in the underlying frontal white matter.

We found large differences in FA and MD values between the cases with CAA and controls (>1 SD), which is in line with findings from in vivo studies.¹⁵ These observations should be interpreted with caution, as several factors related to imaging postmortem brains can influence diffusion properties, including the time interval between death and brain extraction and fixation duration before scanning.^{11,29,30} For example, white matter FA values tend to decrease rapidly within the first days of formalin fixation, but seem to stabilize over longer

Figure 3 Other markers of white matter tissue injury



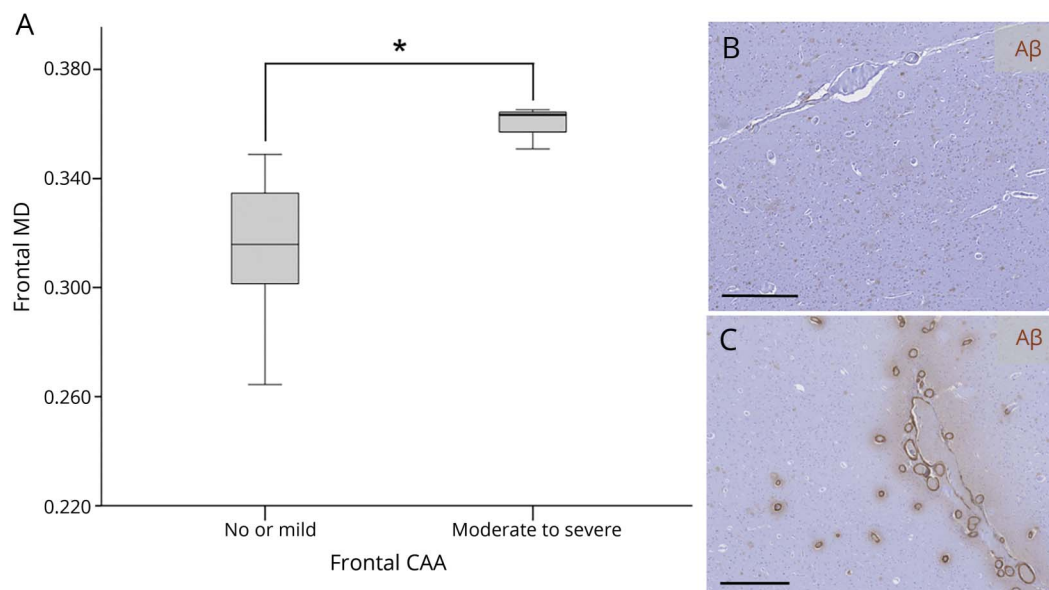
Myelin density and axonal density were measured with fluorescent immunohistochemistry against MBP and NF200 within each region of interest at 40 \times magnification (A). Bright-field immunohistochemistry against GFAP was used to assess gliosis (i.e., GFAP intensity) and reactive astrocyte count (arrows) at 40 \times magnification (B). White matter microinfarcts were assessed on H&E-stained sections (C) and verified with GFAP (inset in D). The microinfarct depicted in C and D (arrow) was found in the medial portion of the inferior longitudinal fasciculus in a case with cerebral amyloid angiopathy. (D) Magnification of the area outlined with a square in C. The inset in D (corresponding to the area outlined with a square) indicates gliosis in the tissue surrounding the microinfarct (the arrow points at a reactive astrocyte). Both scale bars in A and B indicate 50 μ m; scale bar in C indicates 5 mm; and scale bar in D indicates 1 mm. DAPI = 4',6-diamidino-2-phenylindole; GFAP = glial fibrillary acidic protein; H&E = hematoxylin & eosin; MBP = myelin basic protein; NF200 = neurofilament 200.

time periods.^{30,31} Of note, in our dataset, fixation duration did not seem to influence the observed associations, since the results did not markedly alter after adding this variable as a covariate in our models. Moreover, despite the effect of formalin fixation on the diffusion properties, FA measured ex vivo has shown to be linearly related to FA measured in vivo in the same cases,³⁰ suggesting that DTI in ex vivo human tissue can be a reliable derivative of DTI measured in living individuals. Likewise, major fiber tracts can be successfully reconstructed on ex vivo diffusion MRI as shown in the present study and previous studies.^{11,32} Unfortunately, we could not control for postmortem interval in our models, since this variable was not known for 4 of 9 cases. Future studies are needed to address the potential influence of this variable on DTI properties.

This study identified several histopathologic correlates of DTI abnormalities in cases with CAA, including loss of axons and myelin, both contributing to tissue rarefaction (an aggregate measure of tissue loss). Multivariate analysis suggested that FA is most sensitive to loss of white matter tissue caused by degeneration of axons, whereas MD is most sensitive to loss of myelin. These findings suggest parallel but subtly different

forms of white matter injury underlying these 2 major DTI-derived parameters. Gliosis and oligodendrocyte loss do not appear to have substantial roles in CAA-related DTI abnormalities, even though both forms of tissue injury are observed in the white matter of patients with SVD.^{33,34} This further suggests that FA and MD reflect rather specific underlying microstructural changes in patients with CAA, which is informative for inferring pathogenic mechanisms using (longitudinal) DTI in living individuals.

We further found that DTI abnormalities were associated with the presence of microinfarcts in the white matter. Microinfarcts are frequently observed on histopathologic examination of patients with CAA, especially in cortical areas affected by vascular β -amyloid.^{35–37} Of importance, microinfarcts are believed to be major contributors to cognitive decline³⁸ because of their widespread appearance throughout the brain and the fact that they affect surrounding tissue well beyond the lesion core.^{39–41} The significant association between white matter microinfarcts and DTI measures in our study is striking given the low number of microinfarcts observed in the examined white matter areas. It is likely that the contribution of white matter microinfarcts to CAA-related



MD in the anterior portion of the anterior thalamic radiation is higher in cases with moderate to severe CAA ($n = 3$) than in patients with no or mild CAA ($n = 6$) in the frontal cortex (A). An example of a parenchymal CAA severity score in the frontal cortex of 0 (none), as assessed on the A β -stained section (B). An example of a parenchymal CAA severity score in the frontal cortex of 2 (moderate) (C). Both scale bars in B and C indicate 500 μm . Units MD are in $10^{-3} \text{ mm}^2/\text{s}$. A β = β -amyloid; CAA = cerebral amyloid angiopathy; MD = mean diffusivity.

brain injury is much greater than can readily be appreciated by sampling only a few areas of the brain, an important topic for future studies.

DTI alterations in the context of neurologic disease—particularly in SVD—have remained largely unexplored, mainly because of the above-mentioned limitations of ex vivo MRI and the unique nature of intact human brain tissue. One study performed ex vivo DTI and histopathologic examination on samples of the prefrontal white matter of older individuals.² Lower FA of the prefrontal white matter was associated with free-radical injury to myelin and axons, especially in samples containing microvascular infarction.² These results further support microvascular infarction as a possible cause of DTI-related white matter abnormalities. Other notable ex vivo DTI findings are obtained from brains of patients with multiple sclerosis.^{32,42} Two studies found that local variations in FA and MD correlated with histopathologic measures of myelin and axonal density,^{32,42} which is in line with our observations in the context of CAA. In our study, and others,⁴² MD was associated with myelin density independent of axonal density, supporting the significant effect of myelin on the magnitude of diffusivity.

The correlation between higher CAA burden in the frontal cortex and increased MD in the underlying white matter suggests that cortical vascular amyloid buildup may directly affect the integrity of connected tissue. The observation that parenchymal β -amyloid plaques were present in the frontal cortex of all cases with CAA suggests that this association was likely not driven by coexisting Alzheimer pathology. The

pathophysiologic mechanisms underlying the association between CAA and MD remain unclear at this point. CAA appears to cause impairments in vascular reactivity in both humans^{43–45} and animal models^{46–48} highlighting the possibility that the white matter changes reflect ischemic injury. The potential role of cortical microinfarcts in generating white matter disorganization also supports ischemic mechanisms.³⁸

A major strength of this study is the use of high-quality diffusion-weighted imaging data as well as detailed semi-automated histopathologic assessments of 9 cases with a well-characterized form of SVD. Our tract-based selection of white matter regions allowed us to obtain high anatomical correspondence between the ROIs on MRI and pathology. Exact anatomical mapping via coregistration techniques was not possible because of deformation of the tissue after sampling and sectioning, which is a limitation of ex vivo MRI-histopathology studies in general. A second limitation to our study is the small number of control cases available for ex vivo scanning, limiting our statistical power for between-group comparisons. The control cases were significantly older than the CAA cases in this study and had low ABC scores, potentially biasing our results. However, the potential bias attributable to the age difference would be toward the null hypothesis. Third, this was an exploratory study in which we tested multiple hypotheses. This may have resulted in false-positive findings, and as such the correlations should be interpreted with caution. Nevertheless, effect sizes were reasonable and the correlations from secondary models were largely consistent and in line with histopathology findings in patients with SVD.⁴⁹ Fourth, the postmortem interval could

unfortunately not be retrieved for 4 of 9 cases. The time between brain extraction and fixation may have influenced some of the imaging parameters and should ideally be controlled in statistical analyses. Finally, no high-quality DTIs during life from the CAA cases included in this study were available, so we were not able to directly compare our ex vivo DTI findings to in vivo values in the same individuals. Future imaging studies should further investigate associations between in vivo and ex vivo DTI findings in patients with SVD.

These results point to specific histologic features—tissue rarefaction, axonal loss, and myelin loss—as candidate pathogenic mechanisms underlying CAA-related DTI changes. Understanding the histopathologic signature of DTI measures in neurologic disease is instrumental for the interpretation of DTI alterations in the living human brain. This study of the histopathology underlying DTI measures in CAA also highlights the potential importance of white matter ischemia in designing future clinical trials to prevent vascular cognitive impairment.⁵⁰

Author contributions

S.J.v.V. was involved in the conception and design of the study, acquisition and analysis of the data, and writing of the manuscript. Y.D.R. was involved in the conception and design of the study, acquisition and analysis of the data, and writing of the manuscript. A.J.v.d.K. was involved in acquisition of the data and provided critical revisions to the manuscript. A.C. was involved in acquisition of the data and provided critical revisions to the manuscript. G.A.R. was involved in acquisition of the data. A.L. was involved in analysis of the data and provided critical revisions to the manuscript. B.J.B. provided critical revisions to the manuscript and was involved in study funding. M.P.F. was involved in the conception and design of the study and study funding. A.V. was involved in the conception and design of the study and provided critical revisions to the manuscript. S.M.G. was involved in the conception and design of the study, provided critical revisions to the manuscript, and provided study funding.

Acknowledgment

The authors thank Sarah Grill, Dr. John Dewitt, Jose Gonzalez, and Dr. Jie (Jenny) Zhao for excellent technical assistance, and Dr. Brian Edlow for helpful discussions.

Study funding

This work was supported by the NIH (AG26484, NS096730, R21AG046657, and U01NS086625). S.J.v.V. receives funding from the Netherlands Organisation for Scientific Research (Rubicon fellowship 019.153LW.014). Y.D.R. receives funding from Alzheimer Nederland and ZonMw/Memorabel (733050503) and a Young Talent Fellowship from the Brain Center Rudolf Magnus of the University Medical Center Utrecht. The research of A.L. is supported by a VIDI grant from the Netherlands Organisation for Scientific Research (639.072.411).

Disclosure

The authors report no disclosures relevant to the manuscript. Go to Neurology.org/N for full disclosures.

Publication history

Received by *Neurology* May 25, 2018. Accepted in final form October 23, 2018.

References

1. Snyder HM, Corriveau RA, Craft S, et al. Vascular contributions to cognitive impairment and dementia including Alzheimer's disease. *Alzheimers Dement* 2015;11:710–717.
2. Back SA, Kroenke CD, Sherman LS, et al. White matter lesions defined by diffusion tensor imaging in older adults. *Ann Neurol* 2011;70:465–476.
3. Pantoni L. Cerebral small vessel disease: from pathogenesis and clinical characteristics to therapeutic challenges. *Lancet Neurol* 2010;9:689–701.
4. Iadecola C. The pathobiology of vascular dementia. *Neuron* 2013;80:844–866.
5. O'Sullivan M, Morris RG, Huckstep B, et al. Diffusion tensor MRI correlates with executive dysfunction in patients with ischaemic leukoaraiosis. *J Neurol Neurosurg Psychiatry* 2004;75:441–447.
6. van Norden AG, de Laat KF, van Dijk EJ, et al. Diffusion tensor imaging and cognition in cerebral small vessel disease: the RUN DMC study. *Biochim Biophys Acta* 2012;1822:401–407.
7. Baykara E, Gesierich B, Adam R, et al. A novel imaging marker for small vessel disease based on skeletonization of white matter tracts and diffusion histograms. *Ann Neurol* 2016;80:581–592.
8. Beaulieu C. The basis of anisotropic water diffusion in the nervous system—a technical review. *NMR Biomed* 2002;15:435–455.
9. Concha L. A macroscopic view of microstructure: using diffusion-weighted images to infer damage, repair, and plasticity of white matter. *Neuroscience* 2014;276:14–28.
10. Pierpaoli C, Basser PJ. Toward a quantitative assessment of diffusion anisotropy. *Magn Reson Med* 1996;36:893–906.
11. Miller KL, Stagg CJ, Douaud G, et al. Diffusion imaging of whole, post-mortem human brains on a clinical MRI scanner. *Neuroimage* 2011;57:167–181.
12. Vos SB, Jones DK, Viergever MA, Leemans A. Partial volume effect as a hidden covariate in DTI analyses. *Neuroimage* 2011;55:1566–1576.
13. Greenberg SM, Charidimou A. Diagnosis of cerebral amyloid angiopathy: evolution of the Boston criteria. *Stroke* 2018;49:491–497.
14. Salat DH, Smith EE, Tuch DS, et al. White matter alterations in cerebral amyloid angiopathy measured by diffusion tensor imaging. *Stroke* 2006;37:1759–1764.
15. Reijmer YD, Fotiadis P, Martinez-Ramirez S, et al. Structural network alterations and neurological dysfunction in cerebral amyloid angiopathy. *Brain* 2015;138:179–188.
16. Reijmer YD, Fotiadis P, Charidimou A, et al. Relationship between white matter connectivity loss and cortical thinning in cerebral amyloid angiopathy. *Hum Brain Mapp* 2017 Apr 30.
17. McNab JA, Jbabdi S, Deoni SC, Douaud G, Behrens TE, Miller KL. High resolution diffusion-weighted imaging in fixed human brain using diffusion-weighted steady state free precession. *Neuroimage* 2009;46:775–785.
18. Dale AM, Fischl B, Sereno MI. Cortical surface-based analysis. I. segmentation and surface reconstruction. *Neuroimage* 1999;9:179–194.
19. Leemans A, Jeurissen B, Sijbers J, Jones DK. ExploreDTI: a graphical toolbox for processing, analyzing, and visualizing diffusion MR data. *Proc Intl Soc Mag Reson Med* 2009:3537.
20. Vos SB, Tax CM, Luijten PR, Ourselin S, Leemans A, Froeling M. The importance of correcting for signal drift in diffusion MRI. *Magn Reson Med* 2017;77:285–299.
21. Leemans A, Jones DK. The B-matrix must be rotated when correcting for subject motion in DTI data. *Magn Reson Med* 2009;61:1336–1349.
22. Veraart J, Sijbers J, Sunaert S, et al. Weighted linear least squares estimation of diffusion MRI parameters: strengths, limitations, and pitfalls. *Neuroimage* 2013;81:335–346.
23. Basser PJ, Pajevic S, Pierpaoli C, Duda J, Aldroubi A. In vivo fiber tractography using DT-MRI data. *Magn Reson Med* 2000;44:625–632.
24. Hua K, Zhang J, Wakana S, et al. Tract probability maps in stereotaxic spaces: analyses of white matter anatomy and tract-specific quantification. *Neuroimage* 2008;39:336–347.
25. Johnson RT, Yeatman JD, Wandell BA, Buonocore MH, Amaral DG, Nordahl CW. Diffusion properties of major white matter tracts in young, typically developing children. *Neuroimage* 2014;88:143–154.
26. Love S, Chalmers K, Ince P, et al. Development, appraisal, validation and implementation of a consensus protocol for the assessment of cerebral amyloid angiopathy in post-mortem brain tissue. *Am J Neurodegener Dis* 2014;3:19–32.
27. Schindelin J, Arganda-Carreras I, Frise E, et al. Fiji: an open-source platform for biological-image analysis. *Nat Methods* 2012;9:676–682.
28. Cohen J. *Statistical Power Analysis for the Behavioral Sciences*, 2nd ed. Mahwah, NJ: Lawrence Erlbaum Associates; 1988.
29. Shepherd TM, Flint JJ, Thelwall PE, et al. Postmortem interval alters the water relaxation and diffusion properties of rat nervous tissue—implications for MRI studies of human autopsy samples. *Neuroimage* 2009;44:820–826.
30. Wu Y, Dawe RJ, Evia AM, et al. Ex-vivo diffusion anisotropy of human brain hemispheres. *Proc Intl Soc Mag Reson Med* 2016;24:3404.

31. Dyrby TB, Baaré WF, Alexander DC, Jelsing J, Garde E, Søgaard LV. An ex vivo imaging pipeline for producing high-quality and high-resolution diffusion-weighted imaging datasets. *Hum Brain Mapp* 2011;32:544–563.
32. Kolasinski J, Stagg CJ, Chance SA, et al. A combined post-mortem magnetic resonance imaging and quantitative histological study of multiple sclerosis pathology. *Brain* 2012;135:2938–2951.
33. Simpson JE, Fernando MS, Clark L, et al. White matter lesions in an unselected cohort of the elderly: astrocytic, microglial and oligodendrocyte precursor cell responses. *Neuropathol Appl Neurobiol* 2007;33:410–419.
34. Gouw AA, Seewann A, van der Flier WM, et al. Heterogeneity of small vessel disease: a systematic review of MRI and histopathology correlations. *J Neurol Neurosurg Psychiatry* 2011;82:126–135.
35. Kövari E, Herrmann FR, Hof PR, Bouras C. The relationship between cerebral amyloid angiopathy and cortical microinfarcts in brain ageing and Alzheimer's disease. *Neuropathol Appl Neurobiol* 2013;39:498–509.
36. Arvanitakis Z, Capuano AW, Leurgans SE, et al. The relationship of cerebral vessel pathology to brain microinfarcts. *Brain Pathol* 2016;27:77–85.
37. Van Veluw SJ, Charidimou A, Van der Kouwe AJ, et al. Microbleed and microinfarct detection in amyloid angiopathy: a high-resolution MRI-histopathology study. *Brain* 2016;139:3151–3162.
38. Van Veluw SJ, Shih AY, Smith EE, et al. Detection, risk factors, and functional consequences of cerebral microinfarcts. *Lancet Neurol* 2017;16:730–740.
39. Auriel E, Edlow BL, Reijmer YD, et al. Microinfarct disruption of white matter structure: a longitudinal diffusion tensor analysis. *Neurology* 2014;83:182–188.
40. Hinman JD, Lee MD, Tung S, Vinters HV, Carmichael ST. Molecular disorganization of axons adjacent to human lacunar infarcts. *Brain* 2015;138:736–745.
41. Summers PM, Hartmann DA, Hui ES, et al. Functional deficits induced by cortical microinfarcts. *J Cereb Blood Flow Metab* 2017;37:3599–3614.
42. Schmierer K, Wheeler-Kingshott CA, Boulby PA, et al. Diffusion tensor imaging of post mortem multiple sclerosis brain. *Neuroimage* 2007;35:467–477.
43. Dumas A, Dierksen GA, Gurol ME, et al. Functional magnetic resonance imaging detection of vascular reactivity in cerebral amyloid angiopathy. *Ann Neurol* 2012;72:76–81.
44. Peca S, McCreary CR, Donaldson E, et al. Neurovascular decoupling is associated with severity of cerebral amyloid angiopathy. *Neurology* 2013;81:1659–1665.
45. van Opstal AM, van Rooden S, van Harten T, et al. Cerebrovascular function in presymptomatic and symptomatic individuals with hereditary cerebral amyloid angiopathy: a case-control study. *Lancet Neurol* 2017;16:115–122.
46. Shin HK, Jones PB, Garcia-Alloza M, et al. Age-dependent cerebrovascular dysfunction in a transgenic mouse model of cerebral amyloid angiopathy. *Brain* 2007;130:2310–2319.
47. Han BH, Zhou M, Abousaleh F, et al. Cerebrovascular dysfunction in amyloid precursor protein transgenic mice: contribution of soluble and insoluble amyloid-beta peptide, partial restoration via γ -secretase inhibition. *J Neurosci* 2008;28:13542–13550.
48. Park L, Koizumi K, El Jamal S, et al. Age-dependent neurovascular dysfunction and damage in a mouse model of cerebral amyloid angiopathy. *Stroke* 2014;45:1815–1821.
49. Skrobot OA, Attems J, Esiri M, et al. Vascular cognitive impairment neuropathology guidelines (VCING): the contribution of cerebrovascular pathology to cognitive impairment. *Brain* 2016;258:853–863.
50. Greenberg SM, Al-Shahi Salman R, Biessels GJ, et al. Outcome markers for clinical trials in cerebral amyloid angiopathy. *Lancet Neurol* 2014;13:419–428.